Supplementary Information for

Perturbation of Nanoplastics on Biomembranes: Molecular Insights from Neutron Scattering

*Shuo Qian *1, Honghai Zhang 1, Wellington Leite 1, Andrew E. Whitten 2, Piotr Zolnierczuk 1, Yue Yuan 1, Qiu Zhang 1*

1 Oak Ridge National Laboratory, Oak Ridge, TN USA

2 Australian Nuclear Science and Technology Organisation, Lucas Heights, NSW 2234, Australia

***** Corresponding Author

Shuo Qian, Oak Ridge National Laboratory, Oak Ridge, TN

qians@ornl.gov

865-241-1934

Nanoplastics Contrast Matching Point Measurement

Neutron scattering length density (SLD) is a fundamental material property that quantifies the collective neutron scattering power of a molecule per unit molecular volume [1,2]. It is calculated by summing the coherent scattering lengths of all the atoms within a molecule and dividing by the molecular volume. The practical importance of SLD lies in "contrast," as the intensity of scattered neutrons in an experiment (e.g., SANS) is proportional to the square of the SLD difference between different components in a sample, enabling the highlighting of specific structures by manipulating this contrast through isotopic substitution, such as replacing hydrogen with deuterium, at the contrast matching point (CMP).

The scattering profiles at different D_2O ratios (v/v = 0, 40%, 50%, 70%, 90%) were in Fig. S1. From a linear regression of $\sqrt{I}$ vs. D_2O ratio (v/v), the CMP, in terms of D_2O ratio, was determined as where the line intercepts the zero intensity (Fig. 1). Due to constraint of SANS beam time, and the dominant polystyrene composition, only AM PS was measured. The AM functionalization on the NP surface makes a negligible contribution to the SANS signal.

The data fitted well with a sphere model with a radius of 26.8 ± 0.1 nm, accounting for resolution smearing (Fig. S2), confirming the well-defined spherical morphology and the size as measured by DLS in suspension (diameter = 52.6 nm). Note the PDI in DLS was not needed in the fitting as the effect of particle polydispersity is much less significant than the instrument resolution effect.

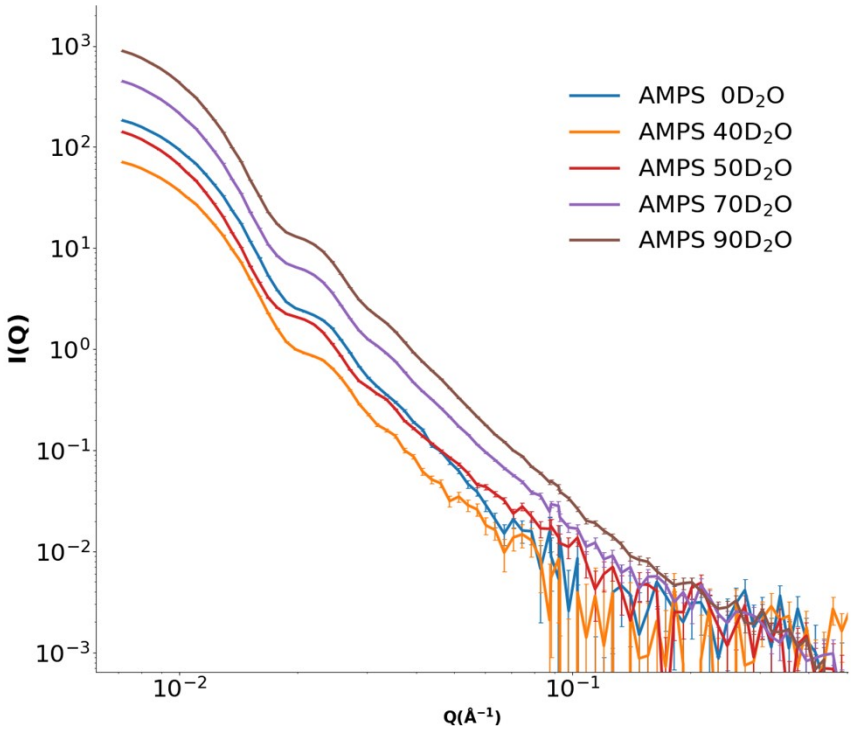

Figure S1. AM PS SANS measured at different D_2O ratios

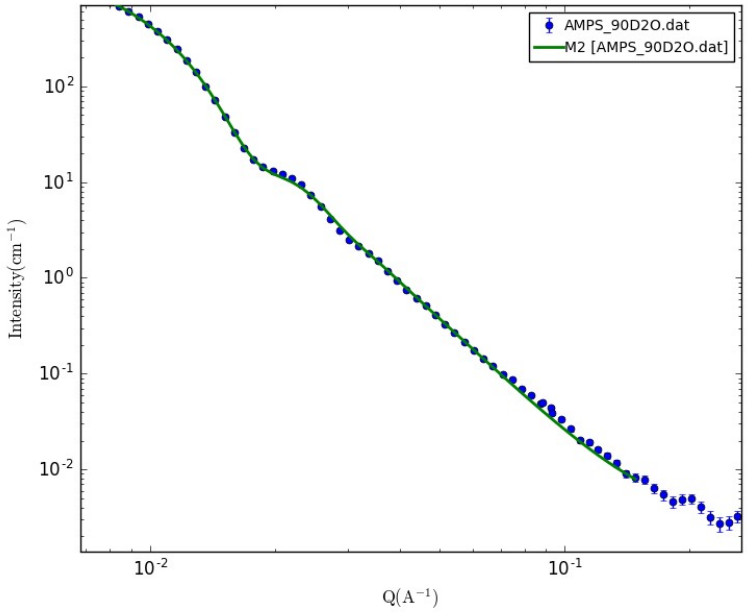

Figure S2. A sphere model fitting of AM PS in 90% D_2O

To further confirm the morphology, diluted nanoparticle suspensions were drop casted on silica surfaces and imaged using a Field Emission Scanning Electron Microscopy (SEM) (Merlin, Zeiss, USA) under 1 kV acceleration voltage. The spherical shapes and uniformity are consistent with DLS and SANS measurements.

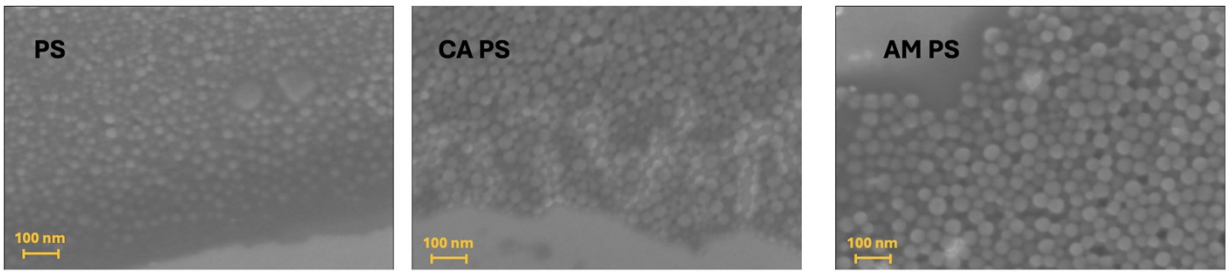

Figure S3. SEM of PS and modified PS nanoparticles

Cryo-EM on LUVs in the presence of PS NPs

The presence of LUVs was verified by Cryo-EM. 3 µL of The DMPC LUV sample with 1% PS was freezed at 22 °C under 100% relative humidity. The cryo-EM viewgraph was taken by a Krios Cryo TEM instrument (Thermo Fisher Scientific). The formation of LUV is evident. However, as mentioned in the main text, the NP-membrane interaction can be disturbed easily during the Cryo-EM sample preparation, the data provided only limited insight into their interaction.

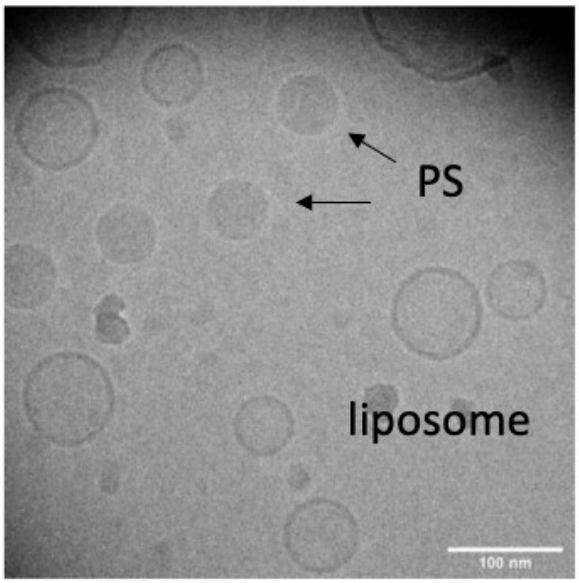

Figure S4. Cryo-EM of DMPC LUVs in the presence of 1% PS.

Additional SANS analysis detail

The lamellar model fitting was performed using SASView (sasview.org), employing its built-in implementation of the model. The SLD for D54-DMPC was set to 6.3×10^{-6} Å^{-2}, and the solvent SLD, corresponding to 26% D_2O, was set to 1.239×10^{-6} Å^{-2}. The fitting was carried out over a Q range of 0.4–4.75 nm^{-1}. Instrumental resolution (the smearing effect) was included using the reported ΔQ values from the instrument, and data weighting was applied based on the experimental uncertainties $\Delta I(Q)$. The parameter uncertainties in SASView were estimated from the square roots of the diagonal elements of the covariance matrix produced by the Levenberg–Marquardt optimizer per its documentation (sasview.org). Here, we report additional model output parameters not included in the main text, along with the corresponding reduced χ^2 values.

Table S1. Additional D54-DMPC data fitting parameters and χ^2 values using the lamellar model

	scale	Background (cm^{-1})	χ^2
DMPC lipid only	0.0107	0.0030	1.85
AM 0.5%	0.0084	0.0114	1.75
AM 1%	0.0043	0.0063	1.29
AM 2%	0.0038	0.0076	1.24
CA 0.5%	0.0125	0.0086	1.70
CA 1%	0.0071	0.0097	1.15
CA 2%	0.0058	0.0061	1.02
PS 0.5%	0.0093	0.0074	1.90
PS 1%	0.0049	0.0076	1.78
PS 2%	0.0005	0.0025	0.89

In fitting the D54-DMPC data, the low-Q region of the AM 2% sample was fitted using the Guinier–Porod function over a Q range of 0.0297–0.5288 nm^{-1}. The fitted parameters are as follows: scale = 6.87, background = –0.16, the radius of gyration R_g = 14.7 nm, the dimension variable s = 0.38, and Porod exponent = 1.93. For the PS 0.5% sample, the low Q Guinier fitting was performed over a Q range of 0.0297–0.3946 nm^{-1}, yielding the following parameters: scale = 51.91, background = 2.49, and R_g = 10.4 nm.

For the *E. coli* data, the SLD for deuterated *E. coli* lipid was set to 6.8×10^{-6} Å^{-2}, and the solvent SLD, corresponding to 26% D_2O, was set to 1.239×10^{-6} Å^{-2}. The fitting was performed over a Q range of 0.5–3 nm^{-1}. It is noted that most of the *E. coli* data were fitted without incorporating thickness polydispersity, while still achieving a moderately acceptable reduced χ^2.

Table S2 Additional *E. coli* data fitting parameters and χ^2 values using the lamellar model. (The Caillè structure factor was included for fitting AM 0.5% data, see the text for details)

	scale	background(cm^{-1})	χ^2
E. coli lipid only	0.0081	0.0047	1.84
AM 0.5%	0.0025	0.0010	1.65
AM 1%	0.0022	0.0015	1.96
AM 2%	0.0024	0.0013	2.10
CA 0.5%	0.0071	0.003	1.93
CA 1%	0.0040	0.0040	1.59
CA 2%	0.0046	0.0018	1.92
PS 0.5%	0.0058	0.0010	1.74
PS 1%	0.0037	0.0027	1.92
PS 2%	0.0018	0.0047	1.64

For the AM 0.5% sample, we modeled the lamellar scattering using the Caillé structure factor [3], which describes stacked lamellae with thermal fluctuations that broaden and reduce Bragg peaks compared to a perfect crystal. The fitted Caillé parameter **(**$0.51)$ indicates moderate fluctuations, consistent with short, flexible stacks. We fixed the number of layers at 4 to reflect the likely finite size of these lamellar aggregates, which produces a single broad peak rather than multiple sharp peaks. The d-spacing of 6.0 nm was determined from the position of this peak, corresponding to the average distance between bilayers. Together, these parameters provide a physically meaningful description of short lamellar stacks with moderate fluctuations and ~6.0 nm repeat spacing.

Additional NSE analysis

Here we present additional NSE analysis to show PS had a fundamental impact on DMPC bilayer compared to other surface modified NPs. However, many of the typical approaches were based on the assumption of bilayer. As a result, in the case of monolayers in the DMPC-PS sample, the values were skewed. Nevertheless, the results consistently showed the drastic changes caused by PS. From the effective bending modulus $\tilde{\kappa}$, the intrinsic bending modulus κ can be derived by

$$\kappa = \tilde{\kappa} \Big/ \left[1 + 48\left(\frac{h}{2h_c}\right)^2\right],$$

where h is the height of the neutral surface from the bilayer midplane, and h_c is the monolayer hydrocarbon thickness. The ratio $\frac{h}{2h_c}$ cannot be measured experimentally, and the ranges differ in the literature. We follow Nagao et al. [4] and use $\frac{h}{2h_c} = 0.5$. Assuming in a thin elastic sheet, the

bending fluctuation leads one leaflet to stretch with the other compressing [4], the bilayer area compressibility modulus K_A is obtained from κ:

$$K_A = \frac{\beta\kappa}{(2h_c)^2}, \tag{8}$$

where β is the coupling constant between the two leaflets ranging from 12 (fully coupled) to 48 (completely uncoupled). Here we use 24 to represent a condition in between [5]. The values of h_c are from the SANS fitting results.

From Fig. S5, both 1% AM and CA NPs change the DMPC bending modulus significantly. AM slightly increases the bending modulus, making the bilayer more rigid even thinning it at the same time. CA softens the bilayer. The results indicate different interaction modalities from positively charged and negatively charged particles, although both manifest as an overall thinning effect. At the same time, the bilayer area compressibility modulus (Fig. S6)—which reflects the energy required to expand or compress the lipid bilayer surface—remains largely unchanged by CA but increases significantly with AM. The most pronounced change is observed in the PS system, where the presence of a monolayer leads to unrealistically low modulus values, indicating that the bilayer assumption no longer holds. This observation is consistent with the SANS structural results.

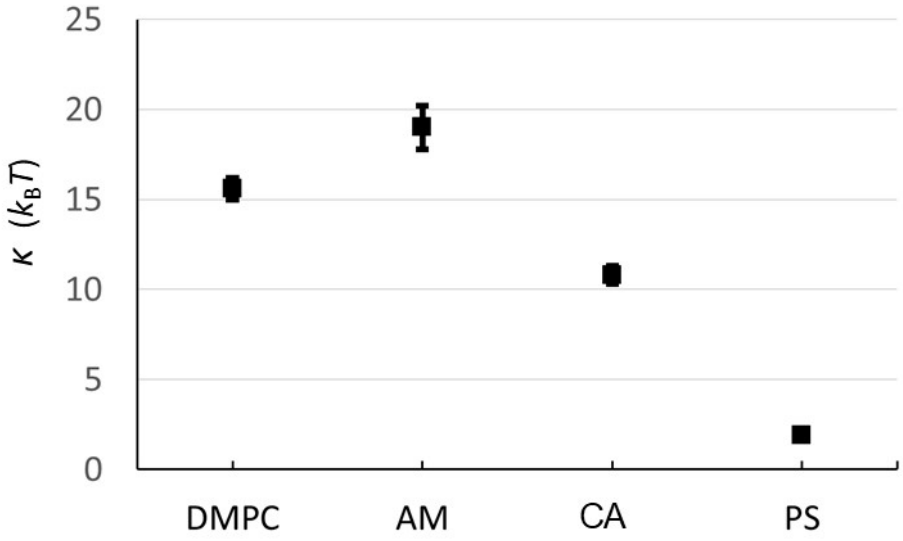

Figure S5. Intrinsic bending modulus for DMPC and with 1% NPs added.

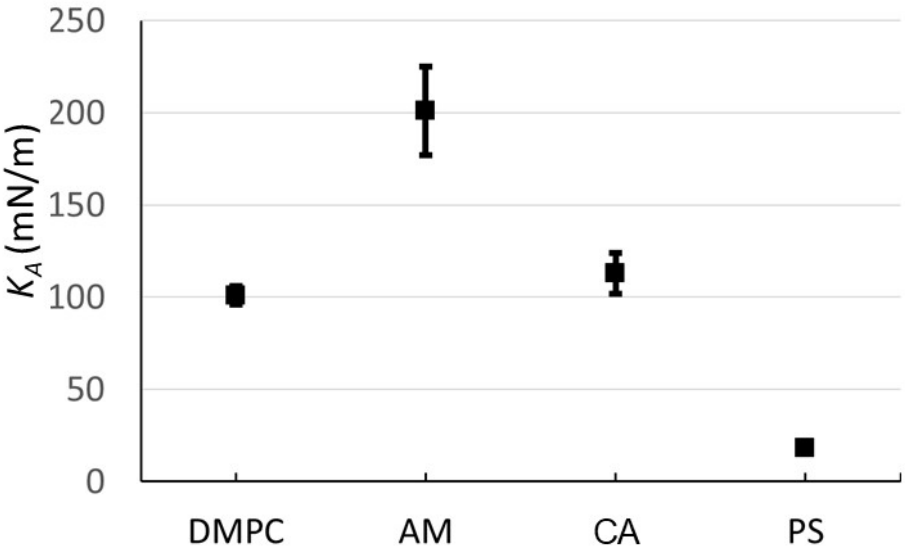

Figure S6. Bilayer area compressibility modulus for DMPC and with 1% NPs added.

References:

[1] S. Qian, V.K. Sharma, L.A. Clifton, Understanding the Structure and Dynamics of Complex Biomembrane Interactions by Neutron Scattering Techniques, Langmuir, 36 (2020) 15189–15211.

[2] B. Chaudhuri, I.G. Muñoz, S. Qian, V.S. Urban, eds., Biological Small Angle Scattering: Techniques, Strategies and Tips, Springer Singapore, 2017.
[3] J. Berghausen, J. Zipfel, P. Lindner, W. Richtering, Influence of Water-Soluble Polymers on the Shear-Induced Structure Formation in Lyotropic Lamellar Phases, J. Phys. Chem. B, 105 (2001) 11081–11088.
[4] M. Nagao, E.G. Kelley, R. Ashkar, R. Bradbury, P.D. Butler, Probing Elastic and Viscous Properties of Phospholipid Bilayers Using Neutron Spin Echo Spectroscopy, J. Phys. Chem. Lett., 8 (2017) 4679–4684.
[5] W. Rawicz, K.C. Olbrich, T. McIntosh, D. Needham, E. Evans, Effect of Chain Length and Unsaturation on Elasticity of Lipid Bilayers, Biophysical Journal, 79 (2000) 328–339.